# Adipocytes reprogram carbon and nitrogen metabolism to maintain lipogenic flux in the absence of *Bckdha*

Courtney R. Green[1,2,5], Karl A. Wessendorf-Rodriguez[1,2], Rory Turner[3], Justin D. Hover[2], Anne N. Murphy[4], Martina Wallace[3]*, Christian M. Metallo[1,2]*

**Affiliations:**

1. Molecular and Cellular Biology Laboratory, Salk Institute for Biological Studies, 10010 N. Torrey Pines Rd., La Jolla, CA, USA 92037
2. Department of Bioengineering, University of California, San Diego, 9500 Gilman Drive, La Jolla, CA, USA 92093
3. School of Agriculture and Food Science, University College Dublin, Belfield, Dublin 4, Ireland
4. Department of Pharmacology, University of California, San Diego, 9500 Gilman Drive, La Jolla, CA, USA 92093
5. Present address: Dexcom, Inc., 6340 Sequence Dr., San Diego, CA, USA 92121

* To whom correspondence should be addressed:

Martina Wallace (martina.wallace@ucd.ie, +353 1 7166932) and Christian M. Metallo (metallo@salk.edu +1 858 453 4100 x1293)

**Abstract**

**Objective**: Adipocytes upregulate branched-chain amino acid (BCAA) catabolism during differentiation, but the downstream metabolic and biological impacts of this induction remain unclear. Here we sought to understand how BCAA catabolism supports intermediary metabolism and function in cultured adipocytes.

**Methods**: Using CRISPR/Cas9 gene-editing, we generated 3T3-L1 pre-adipocytes deficient in either branched-chain ketoacid dehydrogenase, subunit alpha (*Bckdha*) or acyl-CoA dehydrogenase 8 (*Acad8*), which predominantly metabolizes valine-derived isobutyryl-CoA, and examined their metabolism after differentiation. We performed stable-isotope tracing and mass spectrometry, developed a $^{13}$C metabolic flux analysis ($^{13}$C-MFA) model incorporating central carbon metabolism and lipid biosynthesis, and performed RNA-sequencing to further explore functional changes.

**Results**: Generation of polyclonal cultures deficient in *Bckdha* resulted in a 90%+ decrease in [U-$^{13}C_6$]leucine labeling in citrate in differentiated adipocytes ($p<0.001$). Lipid droplet accumulation and mRNA levels of key markers of adipocyte differentiation were unaffected by *Bckdha* deficiency; however, gene set enrichment analysis (GSEA) indicated adipogenesis and glycolysis were the primary downregulated pathways in these cells. *Bckdha*-deficient adipocytes had decreased glucose uptake ($p<0.05$), glycolytic flux ($p<0.05$), and increased glutamine contribution to the TCA cycle ($p<0.05$). These findings were supported by reduced lactate secretion ($p<0.001$) and oxygen consumption rates ($p<0.05$) and correlated with the transcriptional changes observed in adipocytes. Total *de novo* fatty acid synthesis flux was maintained but levels of odd-chain fatty acids and branched-chain fatty acids were reduced, as was the C16:1/C16:0 ratio. $^{13}$C-MFA confirmed these changes and highlighted the complex

relationship between the TCA cycle, BCAA catabolism, and mitochondrial respiration. Finally, *Acad8* deficiency resulted in far fewer differentially expressed genes compared to *Bckdha* deficiency and milder metabolic changes overall.

**Conclusions**: These findings highlight key metabolic and transcriptional changes that occur due to *Bckdha* deficiency in adipocytes and identify important links between BCAA catabolism, glycolytic flux, and respiration.

**Highlights**:

- *Bckdha* deficiency reduced glycolysis and lactate secretion in adipocytes
- Pyruvate and glutamine contribution to TCA metabolism and acetyl-CoA increased
- *de novo* fatty acid synthesis flux was maintained but fatty acid diversity decreased
- RNA-seq data highlighted regulation of genes in glycolysis, adipogenesis, and EMT
- *Acad8* deficiency resulted in fewer altered transcripts and milder metabolic changes

57 **Introduction**

58 The branched-chain amino acids (BCAAs) leucine, isoleucine, and valine are essential amino acids
59 catabolized by a series of mitochondrial enzymes to acetyl-CoA and propionyl-CoA (PropCoA).
60 While diverse tissues use this pathway for energy generation, signaling, and biosynthesis (*1, 2*),
61 adipose tissue is increasingly appreciated as an important contributor to BCAA homeostasis (*3-7*).
62 This pathway is upregulated during the initial stages of adipocyte differentiation (*6-12*) and is
63 highly active in brown adipose tissue where BCAA catabolism is required to maintain
64 thermogenesis in mice (*5*). Catabolism of BCAAs in adipocytes is initiated by mitochondrial
65 BCAT2, which transfers the amino nitrogen to α-ketoglutarate yielding glutamate and a
66 corresponding branched-chain α-keto acid (BCKA). These BCKAs are subsequently oxidized by
67 the branched-chain ketoacid dehydrogenase (BCKD) complex, a highly regulated, rate-limiting
68 step in BCAA catabolism, which decarboxylates the BCKA, covalently adds a coenzyme A
69 moiety, and yields a short branched-chain fatty acyl-CoA (SBCFA-CoA). A series of enzymatic
70 steps further catabolize SBCFA-CoAs to acetyl-CoA and propionyl-CoA, with the latter serving
71 as an anaplerotic substrate for the tricarboxylic acid cycle upon conversion to methylmalonyl-CoA
72 in an adenosylcobalamin-dependent reaction. Alternatively, SBCFA-CoAs and other pathway
73 intermediates are exported to the cytosol to act as signaling molecules or substrates for fatty acid
74 synthase (FASN), which results in formation of iso- or anteiso-monomethyl branched-chain fatty
75 acids (BCFAs) (*13-16*).

76

77 Elevated circulating BCAAs are emerging as a hallmark of metabolic syndrome (*17-19*) and
78 insulin resistance and obesity are associated with systemic dysregulation of BCAA metabolism
79 (*1*). Transcriptional and proteomic studies of white adipose tissue in humans indicate obesity and

80 insulin resistance significantly suppress BCAA catabolism in this tissue (*12, 20*). *In vitro* studies
81 have shown that hypoxic stress potently downregulates flux through BCAA catabolism in
82 adipocytes (*13*) and recent studies in humans found BCAA catabolic gene expression positively
83 correlates with oxygen tension in humans (*21*). This indicates obesity-induced hypoxia may
84 mediate the observed defects in BCAA catabolism in obese adipose tissue. Given the plasticity
85 of adipose tissue (*22, 23*) with an estimated 10% annual turnover of adipocytes (*24*), there is a
86 need to understand how suppression of BCAA catabolism during differentiation due to the obese
87 microenvironment may impact differentiation and function. Previous *in vitro* studies have found
88 that shRNA mediated knockdown of branched-chain ketoacid dehydrogenase, subunit alpha
89 (*Bckdha*) (*10*), the leucine catabolic enzyme methylcrotonoyl-CoA carboxylase 1 (*Mccc1*) (*6*) or
90 siRNA-mediated knockdown of 3-hydroxyisobutyryl-CoA hydrolase (*Hibch*) (*25*) throughout
91 differentiation decreased lipid accumulation indicating impaired differentiation. *In vivo*,
92 knockout of *Bcat2* in white adipocytes induces interscapular white adipose tissue (iWAT)
93 browning (*15*) whereas disruption of BCAA catabolism in brown adipose tissue via knockout of
94 the mitochondrial BCAA transporter *Slc25a44* or *Bckdha* impairs thermogenesis (*5, 26*).
95 Collectively, these data indicate altered BCAA catabolism significantly impacts adipocyte
96 function but a comprehensive assessment of how this impacts flux through other pathways in
97 central carbon metabolism is lacking.
98
99 Defects in BCAA catabolism also define certain Mendelian disorders such as maple syrup urine
100 disease (MSUD) which present with diverse neurological and growth phenotypes (*27, 28*). For
101 example, MSUD patients have very little BCKDH complex activity, which results in elevated
102 levels of BCAAs and BCKAs (*29*). Left untreated, MSUD can cause neurological dysfunction and

103 focal brain injury that results in failure to thrive, seizure, coma, and death within the first weeks
104 of life. Dietary interventions are efficacious for some patients, but chronic neuropsychological
105 problems can persist (*29-33*). Inborn errors of metabolism also exist in the Acad family of
106 enzymes, such as isobutyryl-CoA dehydrogenase deficiency (IBDD). IBDD is caused by
107 mutations in *Acad8* which prevents complete valine catabolism (*34, 35*). In contrast to MSUD,
108 IBDD is often asymptomatic in infants and can remain undiagnosed until a major health event
109 occurs (*36*). As such, key questions remain regarding the biochemical drivers of pathophysiology
110 of such organic acidemias, which could result from changes in the abundance of BCAAs, BCKAs,
111 post-translational modifications, or lipids.
112
113 Here we sought to functionally interrogate the BCAA pathway by engineering cultured 3T3-L1
114 adipocytes to be deficient in *Bckdha* or *Acad8* genes using CRISPR/Cas9. Using stable isotope
115 tracing, mass spectrometry, transcriptomics, and metabolic flux analysis (MFA) modeling, we
116 demonstrate that impairment of BCAA catabolism results in decreased glycolytic flux, lactate
117 secretion, and oxygen consumption. Flux through fatty acid synthase, however, is maintained and
118 this is supported by increased glutamine utilization and increased entry of pyruvate into the TCA
119 cycle. Although lipid droplet accumulation and expression of key adipocyte differentiation
120 markers is not impacted by *Bckdha* or *Acad8* deficiency, gene set enrichment analysis of RNAseq
121 data reveal downregulation of genes associated with adipogenesis, hypoxia, and glycolysis
122 indicating more subtle changes in differentiation and function. In addition, comparison of *Acad8*
123 and *Bckdha* deficiency revealed that *Bckdha* deficiency leads to far more significantly altered
124 pathways at both the transcriptional and metabolic level. These cell metabolism studies provide a

125 detailed roadmap for exploring and understanding the BCAA catabolic pathway and its regulation
126 in adipocytes.
127
128 **Results**
129 *Generation and validation of* Bckdha-*deficient adipocyte cultures*
130 To explore the impact of compromised BCAA catabolism in adipocytes we generated polyclonal
131 cultures of 3T3-L1 pre-adipocytes lacking *Bckdha* using CRISPR/Cas9 (single-guide (sg) Control
132 and *Bckdha*) (Fig 1A). Lipid accumulation appeared unaffected (Fig 1B) and *Bckdha* knockdown
133 was further confirmed with a 90%+ decrease in [U-$^{13}C_6$]leucine labeling to citrate (Fig. 1C). The
134 expression of key adipocyte mRNA differentiation markers was largely unchanged in these
135 polyclonal cultures (Fig. 1D), indicating a minimal impact on differentiation efficiency. However,
136 higher BCAA abundances and an elevated α-ketoisocaproate (KIC)/Leucine ratio were seen in
137 *Bckdha*-deficient adipocytes (Fig. 1E & Supp. Fig. 1A). Uptake of all BCAAs was also
138 significantly reduced (Fig. 1F). As BCAA catabolism can supply nitrogen for amino acid
139 synthesis, we also quantified the net uptake, secretion, or biosynthesis of non-essential amino acids
140 from [U-$^{13}C_6$]glucose. These rates were largely unchanged in *Bckdha*-deficient adipocytes under
141 the nitrogen-replete conditions tested here (Supp. Fig. 1B-C).
142
143 To examine the impact of *Bckdha* deficiency on gene expression in adipocytes, we performed
144 RNAseq on our polyclonal cell populations. We found 887 genes that were significantly
145 differentially expressed (Fig. 2A). These genes included *Scd1* and *Scd2* as well as *Sema3g*, an
146 adipokine recently shown to be essential for adipogenesis and lipogenesis (*37*). To categorize these
147 differentially expressed genes further, we used WEB-based gene set analysis toolkit (WebGestalt)

148 to perform gene set enrichment analysis (GSEA) with the KEGG pathway functional database. We
149 found seven significantly altered pathways with FDR <0.05, which comprised key functional,
150 metabolic, and signaling pathways relevant for adipocyte function, including oxidative
151 phosphorylation, thermogenesis, glycolysis, HIF-1 signaling, and AMPK signaling (Fig. 2B). We
152 also performed GSEA using the MSigDB biological processes hallmark gene sets database.
153 Notably, adipogenesis was the most downregulated pathway in this analysis, and epithelial-to-
154 mesenchymal transition (EMT) was significantly upregulated (Supp. Fig. 2A), further suggesting
155 that *Bckdha* deficiency impacts cellular differentiation state and broader signaling to some extent.
156 Collectively, these results point to an overall downregulation of adipocyte metabolism and
157 impaired function despite the lack of obvious visual signs or consistent reduction in core
158 differentiation markers as measured by qPCR (Fig. 1D). To complement these broad
159 characterizations of secreted metabolites and pathway transcription in *Bckdha*-deficient
160 adipocytes, we next quantified pathway fluxes in greater detail to better understand how the
161 adipocyte metabolic network was rewired in this setting.
162
163 Bckdha-*deficient adipocytes reprogram intermediary metabolism and bioenergetics*
164 Glycolysis/gluconeogenesis was one of the most downregulated pathways in our GSEA of
165 *Bckdha*-deficient adipocytes. In addition, decreased alanine levels (Fig. 1E) indicated a potential
166 reprogramming of glucose metabolism and alternative usage of pyruvate (Fig. 3A). To explore
167 these changes more directly, we quantified glycolytic rates and the lactate/pyruvate ratio in Control
168 and *Bckdha*-deficient adipocytes. Glucose uptake decreased by up to ~25% (Fig. 3B) but we
169 observed a ~50% decrease in lactate secretion in *Bckdha*-deficient adipocytes (Fig. 3C). Indeed, a
170 reduction in the ratio of lactate secretion/glucose uptake (Fig. 3D) and lactate and pyruvate

171 abundances (Fig. 3E) further supported the reduction in glycolysis suggested by our RNAseq
172 analysis.
173
174 Next, we sought to explore TCA metabolism in greater detail, as reduced BCAA catabolism could
175 limit the supply of oxidative substrates supplying mitochondria and drive increased pyruvate
176 oxidation to compensate. Interestingly, all TCA cycle intermediates were significantly decreased
177 in *Bckdha*-deficient adipocytes (Fig. 4A). We also observed a consistent ~20% decrease in both
178 the basal and maximal oxygen consumption rate (Fig. 4B), similar to results in brown adipocytes
179 deficient in the mitochondrial BCAA transporter SLC25A44 (*5*). To determine how impaired
180 BCAA catabolism impacts the use of other carbon sources, we traced adipocytes with [U-
181 $^{13}C_6$]glucose and [U-$^{13}C_5$]glutamine and quantified isotope enrichment in TCA intermediates.
182 Importantly, we observed a slight, but significant increase in mole percent enrichment (MPE) of
183 citrate, α-ketoglutarate (aKG), and succinate from [U-$^{13}C_6$]glucose in *Bckdha*-deficient adipocytes
184 (Fig. 4C), with relatively subtle differences in the isotopologue distribution of citrate (Supp. Fig.
185 2B). MPE from [U-$^{13}C_5$]glutamine was significantly higher in all TCA intermediates except
186 succinate in *Bckdha*-deficient adipocytes (Fig. 4D). In both 3T3-L1 adipocytes and epididymal
187 white adipose tissue (eWAT), leucine and valine alone contribute 3-8% to the total TCA cycle
188 metabolite mole percent enrichment (Fig. 4E). Therefore, it is consistent that ablation of BCAA
189 catabolism in adipocytes is marked by a reduction in mitochondrial respiration and compensatory
190 increases in pyruvate and glutamine entry into the TCA cycle. Importantly, we saw no significant
191 changes in mitochondrial DNA content in 3T3-L1 adipocytes lacking *Bckdha*, indicating that the
192 reduction in respiration is likely not due to reduced mitochondrial number but rather their function
193 (Supp. Fig. 2C).

194 Bckdha *deficiency alters lipogenic acetyl-CoA sourcing and FA diversity*

195 *Bckdha* deficiency prevents the formation of Prop-CoA and SBCFA-CoAs, which contribute to
196 the synthesis of odd-chain fatty acids (OCFAs) and branched-chain fatty acids (BCFAs) (*9, 10,*
197 *13*). As expected, OCFAs and BCFAs were greatly decreased, while the proportion of even chain
198 fatty acids was significantly increased in *Bckdha*-deficient adipocytes (Fig. 5A-B). Isotopomer
199 spectral analysis (ISA) of palmitate labeling from [U-$^{13}C_6$]glucose demonstrated that the
200 contribution of glucose/pyruvate oxidation to the lipogenic acetyl-CoA pool was also significantly
201 increased (Fig. 5C), further highlighting the compensatory increase in glucose metabolism when
202 BCAA catabolism is impaired. ISA modeling also revealed a decrease in newly synthesized
203 OCFAs and a modest increase in the proportion of newly synthesized C16:0 (Fig. 5D). However,
204 the total amount of newly synthesized fatty acids (accounting for both percentage of pool newly
205 synthesized and molar amount of FA) remained unchanged in *Bckdha*-deficient adipocytes (Fig.
206 5E). These results indicate that central carbon metabolism is rewired to sustain FA synthesis (i.e.
207 acetyl-CoA sourcing) and overall abundances.

208

209 RNAseq results also indicated that expression of the desaturase enzymes SCD1 and SCD2 was
210 decreased in *Bckdha*-deficient adipocytes. To this end we calculated the desaturation index (ratio
211 of monounsaturated to saturated FA) in each cell type. While the C18:1/C18:0 ratio was
212 unchanged, the C16:1/C16:0 ratio was significantly decreased in *Bckdha*-deficient adipocytes
213 indicating a decrease in C16:0 desaturation. As both C18:1 and C18:0 are derived more from
214 uptake than synthesis (compared to C16:1 and C16:0), this difference likely reflects a decrease in
215 desaturation activity that is buffered by import of C18:1 from serum in media (Fig. 5F).

216

217 *MFA modeling of* Bckdha-*deficient adipocytes*

218 To gain confidence in the above interpretations we incorporated data from Control and *Bckdha*-
219 deficient adipocytes cultured with either [U-$^{13}C_6$]glucose, [U-$^{13}C_6$]leucine, or [U-$^{13}C_5$]valine for
220 48 hours into a MFA model using INCA (*38*). The network encompassed relevant reactions within
221 glycolysis, TCA metabolism, BCAA oxidation, and fatty acid synthesis, with
222 compartmentalization of several pathways included (Fig. 6A). The model incorporated isotope
223 enrichment data for pyruvate, TCA cycle intermediates, intracellular and extracellular glutamine,
224 intracellular glutamate, leucine, KIC, valine, and fatty acids C15:0, C16:0, and C17:0, as
225 appropriate (Supplementary Table 1). Direct measurements of uptake and secretion fluxes for
226 glucose, lactate, alanine, valine, leucine, glutamate, and glutamine were also included
227 (Supplementary Table 2-3). The model predicts a significant decrease in glucose uptake and both
228 lactate and alanine secretion (Fig 1E & Fig. 3B-C) in 3T3-L1 *Bckdha*-deficient adipocytes. On the
229 other hand, *Bckdha*-deficient adipocytes exhibited a marked increase in pyruvate dehydrogenase
230 (PDH) flux as well as mitochondrial pyruvate cycling, which is consistent with the observed
231 reduction in acetyl-CoA derived from leucine/isoleucine catabolism. We also included FA
232 synthesis in this model, which trended higher but was not significantly different between the cell
233 types despite the noted shift toward palmitate over OCFA and BCFA synthesis in *Bckdha*-deficient
234 adipocytes. Notably, anaplerotic flux of BCAAs to succinyl-CoA was low in all cells, presumably
235 due to the lack of vitamin B12 present in these cultures (*10*). This shift in carbon balancing from
236 BCAA oxidation to glucose/pyruvate oxidation resulted in the model predicting an increase in
237 oxidative TCA cycle flux. Indeed, glutamine contribution to the TCA cycle was also estimated to
238 be increased in *Bckdha*-deficient adipocytes, which also exhibited higher rates of exchange
239 between glutamate and aKG. These results are in agreement with our independent results using

240 [U-$^{13}C_5$]glutamine as a tracer (Fig. 4D), which were not incorporated into the model due to the
241 high exchange with medium glutamine. Additionally, the model predicted an increase in the uptake
242 (56 nmol/well/h vs 45 nmol/well/h) and secretion (43 nmol/well/h vs 39 nmol/well/h) of
243 glutamine, consistent with the increase in labeled glutamine from the [U-$^{13}C_6$]glucose and decrease
244 in total glutamine in the spent media. These findings highlight the broad impact of *Bckdha*
245 deficiency on nitrogen and amino acid metabolism (*39*).
246
247 Acad8 *deficiency impacts anaplerosis and iso-C16:0 BCFA accumulation*
248 In addition to *Bckdha* deficiency, which prevents catabolism of all three BCAAs and downstream
249 pathways, we also investigated the phenotype of adipocytes deficient in *Acad8*, which catalyzes
250 the oxidation of valine-derived isobutyryl-CoA (and thus only blocks valine catabolism). ACAD8
251 protein knockdown (Fig. 7A) did not grossly affect lipid accumulation or adipogenic
252 differentiation (Fig. 7B), as observed with *Bckdha* deficiency (Fig. 1B). However, RNAseq
253 analysis of these *Acad8*-deficient adipocytes found only 65 differentially expressed genes ($q<0.05$)
254 (Fig. 7C), much less than the 887 genes observed in our analysis of *Bckdha*-deficient adipocytes
255 (Fig. 2A). Furthermore, *Acad8* deficiency did not consistently alter TCA cycle intermediate levels
256 (Fig. 7D) or citrate labeling from [U-$^{13}C_6$]glucose (Fig. 7E). While *Acad8* deficiency reduced
257 OCFA levels by about 20% and dramatically increased iso-C16:0 abundance, other fatty acids
258 were not affected (Fig. 7F-G), similar to results obtained with shRNA knockdown (*13*). Overall,
259 these results suggest that *Acad8* deficiency elicits more moderate effects compared to *Bckdha*
260 deficiency, which mirrors the relatively minimal phenotype in humans with IBDD compared to
261 MSUD/*Bckdha* deficiency. Collectively, our studies in cultured adipocytes highlight key pathway
262 alterations that occur when BCAA catabolism is compromised.

263 **Discussion**

264 Here we explored how central carbon metabolism is rebalanced in the absence of BCAA or valine
265 catabolism in cultured 3T3-L1 adipocytes. Upon knockdown of *Bckdha* using CRISPR/Cas9,
266 adipocytes maintain fatty acid biosynthetic flux by increasing pyruvate oxidation, glutamine
267 utilization and consequently TCA flux. Notably, glycolysis, oxygen consumption and fatty acid
268 diversity are reduced as a consequence of decreased BCAA catabolism. Overall, our results
269 suggest that adipocytes retain adequate metabolic plasticity to support their biosynthetic demands
270 in the absence of BCKDH activity.

271

272 Our results suggest that decreased BCKDH activity in adipocytes impacts glycolysis and glucose
273 oxidation in distinct ways. In order to maintain *de novo* lipogenesis in the absence of BCAA
274 catabolism, which can account for 30% lipogenic acetyl-CoA (*10, 13*), cells increase reliance on
275 acetyl-CoA generation from glucose. To support this flux, adipocytes increase pyruvate transport
276 into the mitochondria and oxidation by PDH. This increased utilization of pyruvate for acetyl-CoA
277 does not lead to increased glycolysis. Instead, glycolytic flux is decreased and lactate secretion is
278 significantly suppressed to enable increased channeling of pyruvate to the mitochondria. Although
279 we could not resolve cytosolic from mitochondrial malic enzyme flux, these results highlight the
280 importance of pyruvate cycling, as cytosolic malic enzyme is a major producer of lipogenic
281 NADPH in adipocytes (*40, 41*). Interestingly, our MFA model estimated oxidative TCA cycle
282 flux to be higher in *Bckdha*-deficient adipocytes (Fig. 6A), despite the reduced oxygen
283 consumption measured independently in these cells (Fig. 4B). Various factors could account for
284 this difference, including an expected increase in the NADH/$FADH_2$ ratio generated by pyruvate-
285 and glutamine-driven TCA flux versus BCAA catabolism. The increased NADH/$FADH_2$ ratio will

286 increase flux through NADH-driven complex I of the electron transport chain. As the P/O ratio
287 (ATP produced per oxygen atom reduced) of NADH is greater than that of $FADH_2$, the cell may
288 be able to meet ATP demands using less oxygen. This potential shift to Complex I-driven
289 respiration is also reflected in the RNAseq gene expression results, where *mt-Nd4,* encoding a
290 complex I subunit, is one of the most upregulated genes in the *Bckdha*-deficient cells.
291
292 Lipid droplet accumulation was not impacted in our polyclonal *Bckdha*-deficient adipocytes,
293 which contrasts our prior results targeting *Bckdha* using shRNA (*10*) and those of others utilizing
294 shRNA or siRNA to alter MCCC1 and HIBCH levels (*6, 25*). However, RNAseq analysis found
295 that adipogenesis was the most downregulated pathway using the molecular signatures database.
296 Increased expression of genes associated with epithelial-to-mesenchymal transition also indicated
297 impaired cellular functional state and differentiation (Supp. Fig. 2B). While our analysis focused
298 on metabolic changes with BCKDH deficiency, our RNAseq results indicate that it may also have
299 broader impacts on cell identity and further studies are needed.
300
301 These cell-based studies provide insights into the broader metabolic changes associated with
302 organic acidemias of the BCAA catabolic pathway, particularly in adipose tissue. Many of these
303 changes are likely to result directly due to a decrease in BCAA-derived carbon and associated
304 reducing equivalents generated from their catabolism. However, *Bckdha* deficiency can also result
305 in elevated BCKAs, and several studies implicate elevated BCKAs but not BCAAs in alterations
306 such as impaired insulin signaling (*42*), reduced TCA cycle intermediate abundances (*43*), and
307 reduced mitochondrial OCR (*44, 45*). Notably, *Bckdha* deficiency induced much broader changes
308 in metabolism and gene expression than *Acad8* deficiency, where valine-mediated anaplerosis was

309 reduced and iso-C16:0 BCFA increased dramatically without grossly altering intermediary
310 metabolism or gene expression. While aberrant accumulation of BCFAs can cause deleterious
311 effects (*46*), these results generally correlate with the higher severity of symptoms in patients with
312 MSUD versus IBDD (*28*). However, endogenous production of BCFAs is blocked in *Bckdha*-
313 deficient adipocytes, similar to reductions observed in obese adipose tissue (*13, 47, 48*) and
314 circulating levels in children with fatty liver (*49*). BCFAs are incorporated into diverse lipid
315 species, which could influence membrane fluidity and associated signaling or metabolic processes
316 (*13, 50-52*). Collectively, these results further highlight the diverse metabolic pathways impacted
317 downstream of BCAA catabolism in adipocytes that warrant further exploration.
318

319 **Acknowledgments**

320 We thank all members of the Metallo laboratory for support and helpful discussions. This study
321 was supported, in part, by US National Institutes of Health (NIH) grants R01CA234245
322 (C.M.M.). M.W. and R.T. are supported by an Ad Astra fellowship. This publication includes
323 data generated at the UC San Diego IGM Genomics Center utilizing an Illumina NovaSeq 6000
324 that was purchased with funding from a National Institutes of Health SIG grant (#S10
325 OD026929). We would also like to thank Dr. Yan Wu for guidance in RNAseq analysis.
326

327 **Author Contributions**

328 C.R.G., M.W., and C.M.M. conceived and designed the study. K.W.-R. performed MFA
329 analysis. C.R.G. conducted RNAseq analysis and KEGG pathway analysis. R.T. and M.W.
330 conducted MSigDB-based RNAseq analysis. M.W. performed *in vivo* tracing studies. C.R.G. and
331 J.D.H. carried out gene expression analysis. J.D.H. assisted with stable-isotope tracing

332 experiments and GC-MS analysis. A.N.M. provided Seahorse equipment and related training and
333 advice. C.R.G. performed all other experiments. C.R.G., M.W., and C.M.M. wrote the paper
334 with input from all authors.
335
336 **Materials & Methods**
337 **Cell Culture & Differentiation**
338 All reagents were purchased from Sigma-Aldrich unless otherwise noted. All media and sera were
339 purchased from Life Technologies unless otherwise stated. Mouse 3T3-L1 pre-adipocytes were
340 provided by Prof. Alan Saltiel and cultured in high glucose Dulbecco's modified Eagle medium
341 (DMEM) (Life Technologies) supplemented with 10% bovine calf serum (BCS) below 70%
342 confluence. Cells were regularly screened for mycoplasma contamination. For differentiation,
343 10,000 cells/well were seeded onto 12-well plates and allowed to reach confluence (termed Day -
344 1). On Day 0, differentiation was induced with 0.5 mM 3-isobutyl-1-methylxanthine (IBMX), 0.25
345 μM dexamethasone, and 1 μg/ml insulin in DMEM containing 10% FBS. Medium was changed
346 on Day 3 to DMEM + 10% FBS with 1 μg/ml insulin. Day 6, and thereafter, DMEM + 10% FBS
347 was used.
348
349 Isotope tracing was carried out 7d post-induction of differentiation. Cells were incubated in custom
350 DMEM (Hyclone) in which the metabolite specified was replaced with the $^{13}C$- or $^{2}H$-labeled
351 version for 24h unless otherwise specified. Fatty acids were then either calculated as percent total
352 fatty acids and normalized to control conditions or normalized to [$^{2}H_{31}$]Palmitate internal standard
353 and normalized to control conditions.
354

355 **Generation of lentiviral CRISPR/Cas9 KO 3T3-L1 adipocytes**

356 Control, Bckdha, and Acad8 target sequences (Supplementary Table 4) were cloned into the
357 lentiCRISPRv2 plasmid, a gift from Feng Zhang (Addgene plasmid #52961) (*53*). For lentivirus
358 production, 2-2.5 million HEK293FT cells were placed in 10cm tissue culture plates in 2 mL of
359 DMEM (containing 1% penicillin/streptomycin, 10% FBS). 24h later, transfection was performed
360 using Lipofectamine 3000 (Invitrogen) with 1.3µg VSV.G/PMD2.G, 5.3µg of lenti-
361 gag/pol/PCMVR8.2 and 4µg of lentiviral vector. Lentivirus-containing supernatants were
362 harvested 48 and 72h later, combined, and concentrated using Amicon Ultra-15 centrifugal filters,
363 100,000 NMWL (Millipore) following the manufacturer's protocol. 3T3-L1 pre-adipocytes were
364 infected with 7µL of virus in 2mL of medium containing 7.5µg of polybrene in a 35mm cell culture
365 dish. Media was changed the following day and allowed to recover for 24h. Selection was
366 performed using 2µg/mL puromycin. Cells were then plated to 12-well plates for differentiation
367 as described above. Puromycin was removed from the medium beginning on day 0 of
368 differentiation.

369

370 **Western Blots**

371 3T3-L1 adipocytes were lysed in ice-cold RIPA buffer with 1x protease inhibitor (Sigma-Aldrich).
372 25µg total protein was separated on a 10% SDS-PAGE gel for BCKDHA and β-actin, while 50µg
373 total protein was loaded for ACAD8. The proteins were transferred to a nitrocellulose membrane
374 and immunoblotted with anti-BCKDHA (Novus Biologicals NBP1-79616) (1:2,500 dilution),
375 anti-β-Actin (Cell Signaling 4970S) (1:10,000), anti-ACAD8 (Aviva Systems Biology
376 OAAB06085) (1:1,000 dilution). Specific signal was detected with horseradish peroxidase-
377 conjugated secondary antibody goat anti-rabbit (1:2,500-1:10,000) using SuperSignal West Pico

378 Chemiluminescent Substrate (Thermo Scientific) and developed using Blue Devil
379 Autoradiography film (Genesee Scientific) or Bio-Rad Chemidoc XRS+ Imaging device.
380
381 **Extraction of metabolites for GC-MS analysis**
382 For cell culture, polar metabolites and fatty acids were extracted using methanol/water/chloroform
383 with [$^{2}H_{31}$]palmitate and norvaline as lipid and polar internal standards, respectively, and analyzed
384 as previously described (*54*). Briefly, cells were washed twice with saline, quenched with -80C
385 methanol and 4C water containing norvaline, scraped into Eppendorfs, and extracted with
386 chloroform containing [$^{2}H_{31}$]Palmitate. After centrifugation, phases are dried separately. Samples
387 are stored at -20C before analysis by GC-MS.
388
389 **GC-MS analysis**
390 Dried polar metabolites were derivatized in 2% (w/v) methoxyamine hydrochloride (Thermo
391 Scientific) in pyridine and incubated at 37°C for 60 min. Samples were then silylated with N-
392 tertbutyldimethylsilyl-N-methyltrifluoroacetamide (MTBSTFA) with 1% tert-
393 butyldimethylchlorosilane (tBDMCS) (Regis Technologies) at 45°C for 30 min. Polar derivatives
394 were analyzed by GC-MS using a DB-35MS column (30m x 0.25mm i.d. x 0.25µm, Agilent J&W
395 Scientific) installed in an Agilent 7890B gas chromatograph (GC) interfaced with an Agilent
396 5977A mass spectrometer (MS) with an XTR ion source. The dried lower chloroform phase was
397 derivatized to form fatty acid methyl esters (FAMEs) via addition of 500µL 2% $H_2SO_4$ in MeOH
398 and incubation at 50°C for 2h. FAMEs were extracted via addition of 100µL saturated salt solution
399 and 2 500µL hexane washes. These were analyzed using a Select FAME column (100m × 0.25mm
400 i.d.) installed in an Agilent 7890A GC interfaced with an Agilent 5975C MS using the following

401 temperature program: 80°C initial, increase by 20°C/min to 170°C, increase by 1°C/min to 204°C,
402 then 20°C/min to 250°C and hold for 10 min. The percent isotopologue distribution of each fatty
403 acid and polar metabolite was determined and corrected for natural abundance using in-house
404 algorithms adapted from Fernandez et al. (*55*). Mole percent enrichment (MPE) was calculated via
405 the following equation:
406

407 $$\frac{\sum_{i=1}^{n} M_i \cdot i}{n}$$

408

409 **Isotopomer spectral analysis (ISA) of fatty acids**

410 Mass isotopomer distributions were determined by integrating metabolite ion fragments and
411 correcting for natural abundance using in-house algorithms as previously described (*10*). The ISA
412 compares a measured fatty acid isotopomer distribution to one that is simulated using a reaction
413 network for palmitate synthesis, whereby 8 AcCoA molecules are consumed to form one palmitate
414 molecule. Models were also generated for OCFA synthesis, whereby 1 PropCoA and 6-7 AcCoA
415 molecules are consumed to form one OCFA as previously described (*13*). Parameters for the
416 relative enrichment of the lipogenic AcCoA pool from a given [$^{13}$C] tracer and the percentage of
417 fatty acids that are *de novo* synthesized are extracted from a best-fit model using INCA v1.6
418 metabolic flux analysis software package (*38*). The 95% confidence intervals for both parameters
419 were estimated by evaluating the sensitivity of the sum of squared residuals between measured
420 and simulated fatty acid mass isotopomer distributions to small flux variations.

421

422

423

424 **Metabolic Flux Analysis**

425 $^{13}C$ MFA was conducted using INCA, a software package based on elementary metabolite unit
426 (EMU) framework (*38, 56*). Fluxes through the metabolic network comprising of glycolysis, the
427 pentose phosphate pathway, the TCA cycle, BCAA catabolism, and fatty acid synthesis and
428 oxidation were estimated by minimizing the sum of squared residuals between experimental MIDs
429 and extracellular fluxes using nonlinear least squares regression for differentiated 3T3-L1
430 adipocytes traced with [U-$^{13}C_6$]glucose, [U-$^{13}C_5$]valine, [U-$^{13}C_6$]leucine. The best global fit was
431 found after estimating 20 times using random initial guesses for all fluxes in the metabolic network.
432 A $\chi^2$ statistical test was applied to assess the goodness-of-fit using $\alpha$ of 0.01. The 95% confidence
433 intervals for each flux in the metabolic network were estimated by sensitivity analysis due to minor
434 flux variations (*57*). See Supplementary Table 1 for metabolites used in the analysis, below for
435 assumptions, and Supplementary Tables 2-3 for raw flux values.

436

437 $^{13}C$ metabolic flux analysis was conducted under the following assumptions:

438 - Cells were assumed to be at metabolic and isotopic steady state, i.e. intracellular free
439 metabolite pool size and $^{13}C$ enrichments are constant.
440 - Per well extracellular flux of glucose, lactate, glutamine, glutamate, alanine, valine, and
441 leucine were assumed to be constant over the course of the labeling experiments.
442 - Experimental replicates from all three tracers were entered into INCA v2.0 and used
443 simultaneously to estimate fluxes for sgControl and sgBckdha, resulting in tighter
444 confidence intervals.
445 - Cells were assumed to be terminally differentiated and did not divert resources towards
446 biomass synthesis.

447 • Succinate and fumarate are structurally symmetric and can be enzymatically converted to
448 their subsequent products in either configuration.
449 • Labeled $CO_2$ release during decarboxylation reactions is diluted upon release and does
450 not reincorporate during carboxylation reactions.
451 • Separate mitochondrial and cytosolic pools of aspartate, oxaloacetate, malate, fumarate,
452 pyruvate, acetyl-CoA, glutamate, and glutamine were modeled with exchange fluxes for
453 malate, aspartate, glutamate, and glutamine.
454 • Relative branching of glucose flux to the oxidative pentose phosphate pathway (PPP)
455 relative to the glucose uptake flux was set to 0.3%. (*40*)
456

457 **RNA isolation and quantitative RT-PCR analysis**

458 Total RNA was purified from cultured cells using Trizol Reagent (Life Technologies) per the
459 manufacturer's instructions. First-strand cDNA was synthesized from 0.5μg of total RNA using
460 High-capacity cDNA Reverse Transcription Kit with RNase inhibitor (Applied Biosystems)
461 according to the manufacturer's instructions. Individual 10μl SYBR Green real-time PCR
462 reactions consisted of 2μL of diluted cDNA, 5μL of SYBR Green Supermix (Bio-Rad), and 1μL
463 of primer master mix containing each forward and reverse primer at 5μM. For standardization of
464 quantification, ribosomal RNA RPL27 was amplified simultaneously. The PCR was carried out
465 on 96-well plates on a CFX Connect Real time System (Bio-Rad) using a three-stage program
466 provided by the manufacturer: 95°C hot-start for 3 min, 40 cycles of 95°C for 10s and 60°C for
467 30s, followed by a 0.5°C/5 sec meltcurve generation protocol. Gene-specific primers used are
468 listed in Supplementary Table 5.
469

470 **RNA-seq library preparation**

471 Cells were lysed in Trizol and total RNA was extracted per manufacturer's instructions. Stranded
472 RNA-Seq libraries were prepared from polyA-enriched mRNA using the Illumina Stranded
473 mRNA library prep kit. Library construction and sequencing was performed by the University of
474 California San Diego (UCSD) Institute for Genomic Medicine. Libraries were run as PE100 on a
475 NovaSeq S4 to a depth of ~25 million reads.

476

477 **RNASeq Analysis and Gene Set Enrichment Analysis**

478 The Kallisto/Sleuth differential expression pipeline analysis was performed for paired triplicate
479 samples of NT, Bckdha, and Acad8 KO. The index was obtained from Pachter lab Kallisto
480 website "Ensembl Transcriptomes v96", mus_musculus.tar.gz. Kallisto was run for paired-end
481 read quantification with sequence based bias correction (--bias) and 100 bootstraps (*58*).
482 Normalized transcript abundances were further passed into sleuth using R, which were then
483 aggregated to gene level (*59*). Ultimately, a pairwise Wald test was performed to compare
484 sgControl v. sgBckdha and sgControl v. sgAcad8 using sleuth.

485

486 GSEA analysis using the KEGG pathway functional database was performed using WEB-based
487 GEne SeT AnaLysis Toolkit (WebGestalt). A rank score was calculated through multiplication
488 of the q-value with the sign of the fold change of sgBckdha and sgControl adipocytes. Only
489 significantly differentially expressed genes ($q<0.05$) were included in the analysis. Redundancy
490 reduction of the enriched gene sets was set to "All." The MSigDB Hallmarks pathway functional
491 database was downloaded in gene symbol format (http://www.gsea-
492 msigdb.org/gsea/msigdb/collections.jsp) (*60, 61*). As this is a human pathway database, the

493 differentially expressed genes in the present study were first mapped to their human homologs
494 using the publicly available mouse human genome homology database compiled by the mouse
495 genome informatics organization (http://www.informatics.jax.org/downloads/reports/) (*62*).
496 GSEA analysis was then conducted using the WebGestalt platform, using the hallmarks pathway
497 set as a custom database, and the human homologs of the differentially expressed genes ($q<0.05$)
498 in this study and their associated rank score as the input gene list.
499
500 **Respirometry**
501 Respirometry was conducted using a Seahorse XF96E Analyzer. For respiration studies, cells were
502 plated at 5,000 cells/well and maintained in 2μg/mL puromycin-containing media until confluence
503 was reached and differentiation was performed as described above. 8 days after differentiation was
504 initiated, growth medium was replaced with DMEM (Sigma #5030) supplemented with 25mM
505 HEPES, 8mM glucose, 2mM glutamine, and 1 mM pyruvate. Mitochondrial respiration is
506 calculated as the oxygen consumption rate sensitive to 1μM rotenone and 2μM antimycin A.
507 Maximal respiration was calculated as the difference between the maximum respiratory rate in
508 response to 5μM FCCP that was sensitive to antimycin A. Immediately after the experiment, cells
509 were gently washed with PBS and either a) fixed with 4% paraformaldehyde and stained with
510 CyQuant (Life Technologies) to determine cell number for normalization purposes or b)
511 solubilized in RIPA buffer and quantified using BCA assay. Data from n=3 independent
512 experiments is depicted after normalization within each experiment.
513
514
515

516 **Animal study**

517 Animal handling and care followed the NIH Guide for Care and Use of Laboratory Animals. The
518 experimental protocol was approved by the Institutional Animal Care and Use Committee. 5 week
519 old male C57BL/6J mice were obtained from Jackson Laboratories and *ad lib* fed a custom 20%
520 kcal fat diet (TD. 160091) for 15 weeks from 6 weeks of age. Diets and incorporated isotopes were
521 obtained from Envigo Teklad Diets and Cambridge isotopes respectively. For the final 3 weeks,
522 25% of the total valine and leucine in the diet was replaced with [U-$^{13}C_5$-$^{15}N$]valine and [U-$^{13}C_6$-
523 $^{15}N$]leucine so that there was 3 g [U-$^{13}C_5$-$^{15}N$]valine /100 grams protein and 4 g [U-$^{13}C_6$-
524 $^{15}N$]leucine/100 grams protein in both diets. Mice were fasted overnight prior to plasma and tissue
525 collection and samples were immediately snap frozen in liquid $N_2$.

526

527 **Statistical analyses**

528 All experiments were repeated at least 3 times and data from 1 representative experiment is shown.
529 For analyses involving 2 groups, a two-tailed Student's t-test was performed. For analyses with 3
530 groups or more, a one- or two-way ANOVA was performed as appropriate. Dunnett correction for
531 multiple comparisons was performed for all analyses except Seahorse measurements.

532

533 **Figure Legends**

534 **Figure 1. *Bckdha* deficiency alters systemic amino acid metabolism**

535 A. Western blot of BCKDHA and β-ACTIN

536 B. Brightfield images of differentiated Control and sgBckdha adipocytes 7 days post-
537 induction of differentiation (scale bar = 400μm)

538 C. Mole percent enrichment of citrate from [U-$^{13}C_6$]leucine in sgControl and sgBckdha
539 adipocytes.
540 D. Expression of adipocyte differentiation markers normalized to sgControl
541 E. Heat map of the fold change of the abundance of intracellular amino acids in *Bckdha*-
542 deficient adipocytes normalized to sgControl
543 F. Normalized relative uptake of leucine, isoleucine, and valine in Control and *Bckdha*-
544 deficient adipocytes
545 Data are presented as means ± SEM (C, F) or means ± SD (D) with three cellular replicates.
546 One-way ANOVA (C) or two-way ANOVA (D, F) all with Dunnett's correction for multiple
547 comparisons. Significance in all is compared to sgControl. Results are depicted from one
548 representative experiment which was repeated independently at least three times.
549 *p<0.05, **p<0.01, ***p<0.001.
550
551 **Figure 2. *Bckdha* deficiency broadly alters gene expression**
552 A. Volcano plots of differentially expressed genes in *Bckdha*-deficient adipocytes compared
553 to Control adipocytes
554 B. Gene set enrichment analysis of *Bckdha*-deficient adipocytes generated using WEB-
555 based GEne SeT AnaLysis Toolkit (WebGestalt)
556
557 **Figure 3: Glucose metabolism is reprogrammed in *Bckdha*-deficient adipocytes**
558 A. Simplified metabolic map of central carbon metabolism
559 B. Molar amount of glucose uptake in Control or *Bckdha*-deficient adipocytes over 48 hours

560 C. Molar amount of lactate secretion in Control or *Bckdha*-deficient adipocytes over 48
561 hours
562 D. Ratio of lactate secretion to glucose uptake after 48 hours
563 E. Intracellular lactate to pyruvate ratio
564 Data are presented as means ± SD (B-E) with three cellular replicates. One-way ANOVA with
565 Dunnett's correction for multiple comparisons (B-E). Significance in all is compared to
566 sgControl. Results are depicted from one representative experiment which was repeated
567 independently at least three times.
568 *p<0.05, **p<0.01, ***p<0.001.
569
570 **Figure 4: Respiration is negatively impacted by Bckdha deficiency**
571 A. Relative abundance of TCA cycle intermediates in *Bckdha*-deficient adipocytes
572 normalized to sgControl adipocytes
573 B. Normalized oxygen consumption rate of 3T3-L1 Control or *Bckdha*-deficient adipocytes
574 treated with the indicated pharmacological inhibitors (n=3 experiments internally
575 normalized to sgControl)
576 C. Mole percent enrichment (MPE) of TCA cycle intermediates after 48 hours of incubation
577 with [U-$^{13}C_6$]glucose
578 D. MPE of TCA cycle intermediates after 48 hours of incubation with [U-$^{13}C_5$]glutamine
579 E. Normalized MPE from dual [U-$^{13}C_6$]leucine and [U-$^{13}C_5$]valine tracing in cultured 3T3-
580 L1 adipocytes and mice epididymal white adipose tissue (eWAT) after 21 days of labeled
581 chow feeding

582 Data are presented as means ± SEM with six cellular replicates (B), means ± SD with three
583 cellular replicates (C-D), or means ± SEM with seven tissue replicates and three cellular
584 replicates (E). Two-way ANOVA with Dunnett's correction for multiple comparisons (A-D).
585 Significance in all is compared to sgControl. Results are depicted from one representative
586 experiment which was repeated independently at least three times.
587 *p<0.05, **p<0.01, ***p<0.001.
588
589 **Figure 5: Altering BCAA catabolism alters fatty acid diversity**
590 A. Relative fold change in total odd- and even- straight-chain fatty acids in *Bckdha*-deficient
591 3T3-L1 adipocytes normalized to Control adipocytes.
592 B. Relative fold change in total branched-chain fatty acids (BCFAs) in *Bckdha*-deficient
593 3T3-L1 adipocytes normalized to Control adipocytes.
594 C. Contribution of [U-$^{13}C_6$]glucose to the lipogenic AcCoA pool used for *de novo*
595 lipogenesis (DNL)
596 D. Percent of fatty acids derived from *de novo* lipogenesis in Control and *Bckdha*-deficient
597 3T3-L1 adipocytes over 48 hours obtained via isotopomer spectral analysis (ISA).
598 E. Molar amount of indicated fatty acids synthesized over 48 hours obtained by combining
599 individual FA DNL values with pool size
600 F. Desaturation index in Control and *Bckdha*-deficient 3T3-L1 adipocytes
601 Data are presented as means ± SD (A, B, F), means ± 95% C.I. (C-D), and means ± SEM (E)
602 with three cellular replicates. Two-way ANOVA (A-B, F) or one-way ANOVA of the total
603 values (E) all with Dunnett's correction for multiple comparisons and non-overlapping 95% C.I.

604 (C, D). Significance in all is compared to sgControl. Results are depicted from one representative
605 experiment which was repeated independently at least three times.
606 *p<0.05, **p<0.01, ***p<0.001.
607
608 **Figure 6. Metabolic flux analysis reveals significant reprogramming of glycolysis and TCA**
609 **metabolism**
610 A. Map of core MFA model. Values are presented as net flux (exchange flux). Blue text is
611 sgControl, red text is sgBckdha. Blue arrows indicate a flux is decreased in sgBckdha
612 compared to sgControl, while a red arrow indicates an increase in flux in sgBckdha. Bold
613 text indicates significantly different reactions.
614
615 **Figure 7. *Acad8* deficiency impacts anaplerosis and alters OCFA and BCFA accumulation**
616 A. Western blot of ACAD8 and β-ACTIN
617 B. Brightfield images of differentiated Control and sgAcad8 adipocytes 7 days post-
618 induction of differentiation (scale bar = 400μm)
619 C. Volcano plots of differentially expressed genes in *Acad8*-deficient adipocytes compared
620 to Control adipocytes
621 D. Heat map of the fold change of the abundance of intracellular TCA cycle intermediates in
622 *Bckdha*-deficient adipocytes normalized to sgControl
623 E. Citrate mass isotopomer distribution (MID) after 48 hours of incubation with [U-
624 $^{13}C_6$]glucose
625 F. Relative fold change in total odd- and even- straight-chain fatty acids in *Acad8*-deficient
626 3T3-L1 adipocytes normalized to Control adipocytes.

627 G. Relative fold change in total branched-chain fatty acids (BCFAs) in *Acad8*-deficient 3T3-
628 L1 adipocytes normalized to Control adipocytes.
629 Data are presented as means ± SD (E-G) with three cellular replicates. Two-way ANOVA (E-G).
630 Significance in all is compared to sgControl. Results are depicted from one representative
631 experiment which was repeated independently at least three times.
632 *p<0.05, **p<0.01, ***p<0.001.
633
634 **Supplementary Figures**
635 Supplementary Figure 1. *Bckdha* deficiency alters BCKA levels and amino acid metabolism
636 A. Ratio of α-ketoisocaproate (KIC) to leucine in Control and *Bckdha*-deficient adipocytes
637 B. Normalized relative uptake or efflux of amino acids in Control and *Bckdha*-deficient
638 adipocytes
639 C. Mole percent enrichment (MPE) of non-essential amino acids alanine, glycine, serine,
640 proline, aspartate, and glutamine from [U-$^{13}C_6$]glucose
641 Data are presented as means ± SD (A-C) with three cellular replicates. One-way ANOVA (A) or
642 two-way ANOVA (B-C). Significance in all is compared to sgControl. Results are depicted from
643 one representative experiment which was repeated independently at least three times.
644 *p<0.05, **p<0.01, ***p<0.001.
645
646
647
648

649 **Supplementary Figure 2. Bckdha deficiency alters transcription and glucose metabolism**

650 **without affecting mitochondrial number:**

651 A. Gene set enrichment analysis of *Bckdha*-deficient adipocytes generated using WEB-

652 based GEne SeT AnaLysis Toolkit (WebGestalt) using the MsigDB biological processes

653 hallmarks database

654 B. Citrate mass isotopomer distribution (MID) after 48 hours of incubation with [U-

655 $^{13}C_6$]glucose

656 C. Normalized gene expression of mitochondrial DNA markers in Control and *Bckdha*-

657 deficient adipocytes

658 Data are presented as means ± SD (B, C) with three cellular replicates. Two-way ANOVA (B,

659 C). Significance in all is compared to sgControl. Results are depicted from one representative

660 experiment which was repeated independently at least three times.

661 *p<0.05, **p<0.01, ***p<0.001.

662

663 **References**:


664 1. M. D. Neinast *et al.*, Quantitative Analysis of the Whole-Body Metabolic Fate of Branched-Chain
665 Amino Acids. *Cell Metab* **29**, 417-429.e414 (2019).
666 2. P. Nicklin *et al.*, Bidirectional transport of amino acids regulates mTOR and autophagy. *Cell* **136**,
667 521-534 (2009).
668 3. H. A. Zimmerman, K. C. Olson, G. Chen, C. J. Lynch, Adipose transplant for inborn errors of
669 branched chain amino acid metabolism in mice. *Molecular genetics and metabolism* **109**, 345-353
670 (2013).
671 4. M. A. Herman, P. She, O. D. Peroni, C. J. Lynch, B. B. Kahn, Adipose tissue branched chain
672 amino acid (BCAA) metabolism modulates circulating BCAA levels. *The Journal of biological*
673 *chemistry* **285**, 11348-11356 (2010).
674 5. T. Yoneshiro *et al.*, BCAA catabolism in brown fat controls energy homeostasis through
675 SLC25A44. *Nature* **572**, 614-619 (2019).
676 6. E. Zaganjor *et al.*, SIRT4 is an early regulator of branched-chain amino acid catabolism that
677 promotes adipogenesis. *Cell reports* **36**, 109345 (2021).
678 7. A. Halama *et al.*, Metabolic switch during adipogenesis: From branched chain amino acid
679 catabolism to lipid synthesis. *Arch Biochem Biophys* **589**, 93-107 (2016).
680 8. D. T. Chuang, C. W. Hu, M. S. Patel, Induction of the branched-chain 2-oxo acid dehydrogenase
681 complex in 3T3-L1 adipocytes during differentiation. *The Biochemical journal* **214**, 177-181
682 (1983).
683 9. S. B. Crown, N. Marze, M. R. Antoniewicz, Catabolism of Branched Chain Amino Acids
684 Contributes Significantly to Synthesis of Odd-Chain and Even-Chain Fatty Acids in 3T3-L1
685 Adipocytes. *PLOS ONE* **10**, (2015).
686 10. C. R. Green *et al.*, Branched-chain amino acid catabolism fuels adipocyte differentiation and
687 lipogenesis. *Nature chemical biology* **12**, 15-21 (2016).
688 11. N. Y. Kedishvili, K. M. Popov, J. A. Jaskiewicz, R. A. Harris, Coordinated expression of valine
689 catabolic enzymes during adipogenesis: analysis of activity, mRNA, protein levels, and metabolic
690 consequences. *Archives of biochemistry and biophysics* **315**, 317-322 (1994).
691 12. D. E. Lackey *et al.*, Regulation of adipose branched-chain amino acid catabolism enzyme
692 expression and cross-adipose amino acid flux in human obesity. *American journal of physiology.*
693 *Endocrinology and metabolism* **304**, 87 (2013).
694 13. M. Wallace *et al.*, Enzyme promiscuity drives branched-chain fatty acid synthesis in adipose
695 tissues. *Nature Chemical Biology* **14**, 1021 (2018).
696 14. C. Jang *et al.*, A branched-chain amino acid metabolite drives vascular fatty acid transport and
697 causes insulin resistance. *Nat Med* **22**, 421-426 (2016).
698 15. Q. X. Ma *et al.*, BCAA-BCKA axis regulates WAT browning through acetylation of PRDM16.
699 *Nat Metab* **4**, 106-122 (2022).
700 16. S. Trefely *et al.*, Quantitative subcellular acyl-CoA analysis reveals distinct nuclear metabolism
701 and isoleucine-dependent histone propionylation. *Mol Cell* **82**, 447-462.e446 (2022).
702 17. C. B. Newgard *et al.*, A branched-chain amino acid-related metabolic signature that differentiates
703 obese and lean humans and contributes to insulin resistance. *Cell metabolism* **9**, 311-326 (2009).
704 18. T. J. Wang *et al.*, Metabolite profiles and the risk of developing diabetes. *Nature medicine* **17**,
705 448-453 (2011).
706 19. M. Guasch-Ferré *et al.*, Metabolomics in Prediabetes and Diabetes: A Systematic Review and
707 Meta-analysis. *Diabetes Care* **39**, 833-846 (2016).
708 20. M. M. Boulet *et al.*, Alterations of plasma metabolite profiles related to adipose tissue distribution
709 and cardiometabolic risk. *Am J Physiol Endocrinol Metab* **309**, E736-746 (2015).
710 21. V. Cifarelli *et al.*, Decreased adipose tissue oxygenation associates with insulin resistance in
711 individuals with obesity. *J Clin Invest* **130**, 6688-6699 (2020).
712 22. W. Sun, S. Modica, H. Dong, C. Wolfrum, Plasticity and heterogeneity of thermogenic adipose
713 tissue. *Nat Metab* **3**, 751-761 (2021).

714 23. A. Sakers, M. K. De Siqueira, P. Seale, C. J. Villanueva, Adipose-tissue plasticity in health and
715 disease. *Cell* **185**, 419-446 (2022).
716 24. K. L. Spalding *et al.*, Dynamics of fat cell turnover in humans. *Nature* **453**, 783-787 (2008).
717 25. M. S. Nilsen *et al.*, 3-Hydroxyisobutyrate, A Strong Marker of Insulin Resistance in Type 2
718 Diabetes and Obesity That Modulates White and Brown Adipocyte Metabolism. *Diabetes* **69**,
719 1903-1916 (2020).
720 26. T. Yoneshiro *et al.*, Metabolic flexibility via mitochondrial BCAA carrier SLC25A44 is required
721 for optimal fever. *Elife* **10**, (2021).
722 27. L. C. Burrage, S. C. S. Nagamani, P. M. Campeau, B. H. Lee, Branched-chain amino acid
723 metabolism: from rare Mendelian diseases to more common disorders. *Human Molecular*
724 *Genetics* **23**, R1-8 (2014).
725 28. I. Knerr, N. Weinhold, J. Vockley, K. M. Gibson, Advances and challenges in the treatment of
726 branched-chain amino/keto acid metabolic defects. *J Inherit Metab Dis* **35**, 29-40 (2012).
727 29. K. A. Strauss, D. H. Morton, Branched-chain Ketoacyl Dehydrogenase Deficiency: Maple Syrup
728 Disease. *Current treatment options in neurology* **5**, 329-341 (2003).
729 30. S. Schönberger, B. Schweiger, B. Schwahn, M. Schwarz, U. Wendel, Dysmyelination in the brain
730 of adolescents and young adults with maple syrup urine disease. *Molecular Genetics and*
731 *Metabolism* **82**, 69-75 (2004).
732 31. J. Korein, C. Sansaricq, M. Kalmijn, J. Honig, B. Lange, Maple syrup urine disease: clinical,
733 EEG, and plasma amino acid correlations with a theoretical mechanism of acute neurotoxicity. *Int*
734 *J Neurosci* **79**, 21-45 (1994).
735 32. D. H. Morton, K. A. Strauss, D. L. Robinson, E. G. Puffenberger, R. I. Kelley, Diagnosis and
736 treatment of maple syrup disease: a study of 36 patients. *Pediatrics* **109**, 999-1008 (2002).
737 33. J. Y. Lee *et al.*, Maple syrup urine disease (MSUD)--clinical profile of 47 Filipino patients. *J*
738 *Inherit Metab Dis* **31 Suppl 2**, S281-285 (2008).
739 34. T. V. Nguyen *et al.*, Identification of isobutyryl-CoA dehydrogenase and its deficiency in
740 humans. *Mol Genet Metab* **77**, 68-79 (2002).
741 35. J. W. Yun *et al.*, A novel ACAD8 mutation in asymptomatic patients with isobutyryl-CoA
742 dehydrogenase deficiency and a review of the ACAD8 mutation spectrum. *Clin Genet* **87**, 196-
743 198 (2015).
744 36. S. Santra, A. Macdonald, M. A. Preece, R. K. Olsen, B. S. Andresen, Long-term outcome of
745 isobutyryl-CoA dehydrogenase deficiency diagnosed following an episode of ketotic
746 hypoglycaemia. *Molecular Genetics and Metabolism Reports* **10**, 28-30 (2017).
747 37. M. Liu *et al.*, Mechanism of SEMA3G knockdown-mediated attenuation of high-fat diet-induced
748 obesity. *J Endocrinol* **244**, 223-236 (2020).
749 38. J. D. Young, INCA: a computational platform for isotopically non-stationary metabolic flux
750 analysis. *Bioinformatics* **30**, 1333-1335 (2014).
751 39. M. M. Islam *et al.*, A novel branched-chain amino acid metabolon. Protein-protein interactions in
752 a supramolecular complex. *J Biol Chem* **282**, 11893-11903 (2007).
753 40. L. Liu *et al.*, Malic enzyme tracers reveal hypoxia-induced switch in adipocyte NADPH pathway
754 usage. *Nature chemical biology* **12**, 345-352 (2016).
755 41. E. H. Oates, M. R. Antoniewicz, Coordinated reprogramming of metabolism and cell function in
756 adipocytes from proliferation to differentiation. *Metab Eng* **69**, 221-230 (2022).
757 42. M. Zhou *et al.*, Targeting BCAA Catabolism to Treat Obesity-Associated Insulin Resistance.
758 *Diabetes* **68**, 1730-1746 (2019).
759 43. J. Wang *et al.*, BCAA Catabolic Defect Alters Glucose Metabolism in Lean Mice. *Front Physiol*
760 **10**, 1140 (2019).
761 44. D. Biswas *et al.*, Branched-chain ketoacid overload inhibits insulin action in the muscle. *J Biol*
762 *Chem* **295**, 15597-15621 (2020).
763 45. H. Sun *et al.*, Catabolic Defect of Branched-Chain Amino Acids Promotes Heart Failure.
764 *Circulation* **133**, 2038-2049 (2016).

46. Y. Kishimoto, M. Williams, H. W. Moser, C. Hignite, K. Biermann, Branched-chain and odd-numbered fatty acids and aldehydes in the nervous system of a patient with deranged vitamin B 12 metabolism. *Journal of lipid research* **14**, 69-77 (1973).
47. X. Su *et al.*, Adipose tissue monomethyl branched-chain fatty acids and insulin sensitivity: Effects of obesity and weight loss. *Obesity* **23**, 329-334 (2014).
48. A. Mika *et al.*, A comprehensive study of serum odd- and branched-chain fatty acids in patients with excess weight. *Obesity* **24**, 1669-1676 (2016).
49. M. C. Sawh *et al.*, Dairy Fat Intake, Plasma Pentadecanoic Acid, and Plasma Iso-heptadecanoic Acid Are Inversely Associated With Liver Fat in Children. *J Pediatr Gastroenterol Nutr* **72**, e90-e96 (2021).
50. R. Mercier, P. Domínguez-Cuevas, J. Errington, Crucial Role for Membrane Fluidity in Proliferation of Primitive Cells. *Cell Reports* **1**, 417-423 (2012).
51. I. Budin *et al.*, Viscous control of cellular respiration by membrane lipid composition. *Science* **362**, 1186-1189 (2018).
52. L. Liu *et al.*, Human fetal intestinal epithelial cells metabolize and incorporate branched chain fatty acids in a structure specific manner. *Prostaglandins Leukot Essent Fatty Acids* **116**, 32-39 (2017).
53. N. E. Sanjana, O. Shalem, F. Zhang, Improved vectors and genome-wide libraries for CRISPR screening. *Nature Methods* **11**, 783-784 (2014).
54. T. Cordes, C. M. Metallo, in *High-Throughput Metabolomics: Methods and Protocols,* A. D'Alessandro, Ed. (Springer New York, New York, NY, 2019), pp. 219-241.
55. C. A. Fernandez, C. Des Rosiers, S. F. Previs, F. David, H. Brunengraber, Correction of 13C mass isotopomer distributions for natural stable isotope abundance. *J Mass Spectrom* **31**, 255-262 (1996).
56. J. D. Young, J. L. Walther, M. R. Antoniewicz, H. Yoo, G. Stephanopoulos, An elementary metabolite unit (EMU) based method of isotopically nonstationary flux analysis. *Biotechnol Bioeng* **99**, 686-699 (2008).
57. M. R. Antoniewicz, J. K. Kelleher, G. Stephanopoulos, Determination of confidence intervals of metabolic fluxes estimated from stable isotope measurements. *Metab Eng* **8**, 324-337 (2006).
58. N. L. Bray, H. Pimentel, P. Melsted, L. Pachter, Near-optimal probabilistic RNA-seq quantification. *Nat Biotechnol* **34**, 525-527 (2016).
59. H. Pimentel, N. L. Bray, S. Puente, P. Melsted, L. Pachter, Differential analysis of RNA-seq incorporating quantification uncertainty. *Nat Methods* **14**, 687-690 (2017).
60. A. Subramanian *et al.*, Gene set enrichment analysis: a knowledge-based approach for interpreting genome-wide expression profiles. *Proc Natl Acad Sci U S A* **102**, 15545-15550 (2005).
61. V. K. Mootha *et al.*, PGC-1alpha-responsive genes involved in oxidative phosphorylation are coordinately downregulated in human diabetes. *Nat Genet* **34**, 267-273 (2003).
62. C. J. Bult *et al.*, Mouse Genome Database (MGD) 2019. *Nucleic Acids Res* **47**, D801-D806 (2019).

## Figure 1
## Bckdha deficiency alters systemic amino acid metabolism

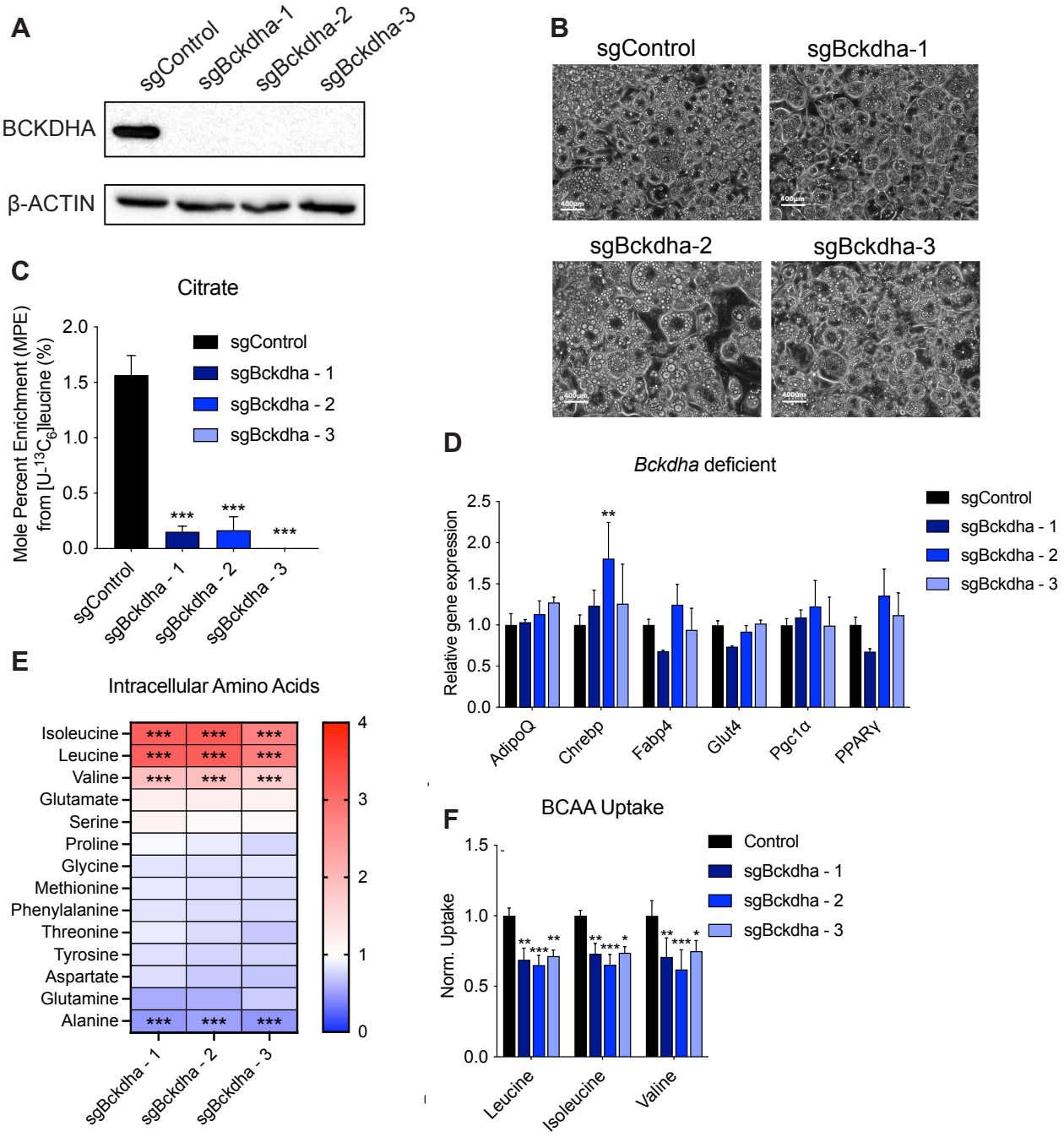


A. Western blot of Bckdha and Actin
B. Brightfield images of differentiated Control and sgBckdha adipocytes 7 days post-induction of differentiation (scale bar = 400μm)
C. Mole percent enrichment of citrate from [U-13C6]leucine in sgControl and sgBckdha adipocytes.
D. Expression of adipocyte differentiation markers normalized to sgControl
E. Heat map of the fold change of the abundance of intracellular amino acids in Bckdha-*deficient* adipocytes normalized to sgControl
F. Normalized relative uptake of leucine, isoleucine, and valine in Control and Bckdha-*deficient* adipocytes

Data are presented as means ± SEM (C, F) or means ± SD (D) with three cellular replicates. One-way ANOVA (C) or two-way ANOVA (D-F) all with Dunnett's correction for multiple comparisons. Significance in all is compared to sgControl. Results are depicted from one representative experiment which was repeated independently at least three times. *p<0.05, **p<0.01, ***p<0.001.

## Figure 2
## Bckdha deficiency broadly alters gene expression

**A**

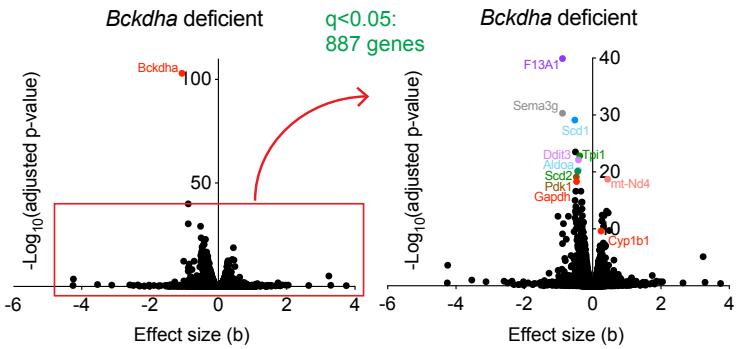


**B**

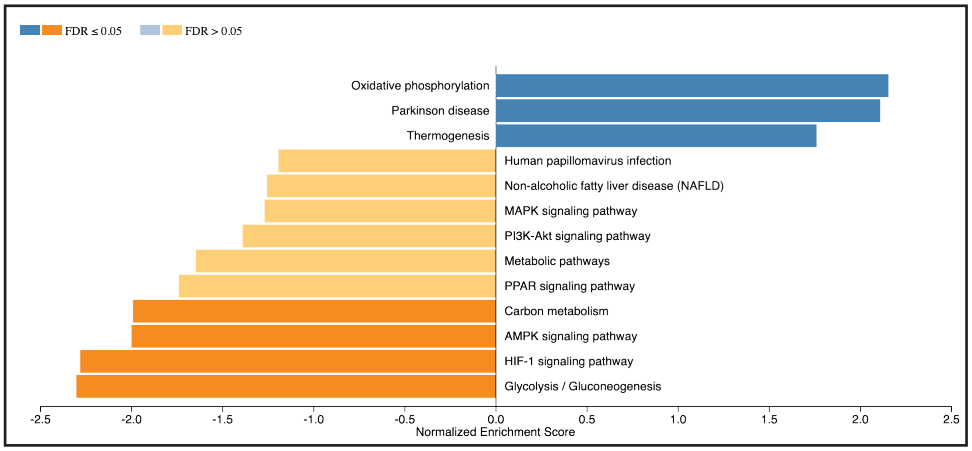


A. Volcano plots of differentially expressed genes in Bckdha-deficient adipocytes compared to Control adipocytes
B. Gene set enrichment analysis of Bckdha deficient adipocytes generated using WEB-based GEne SeT AnaLysis Toolkit (WebGestalt)

## Figure 3
## Glucose metabolism is reprogrammed in Bckdha deficient adipocytes

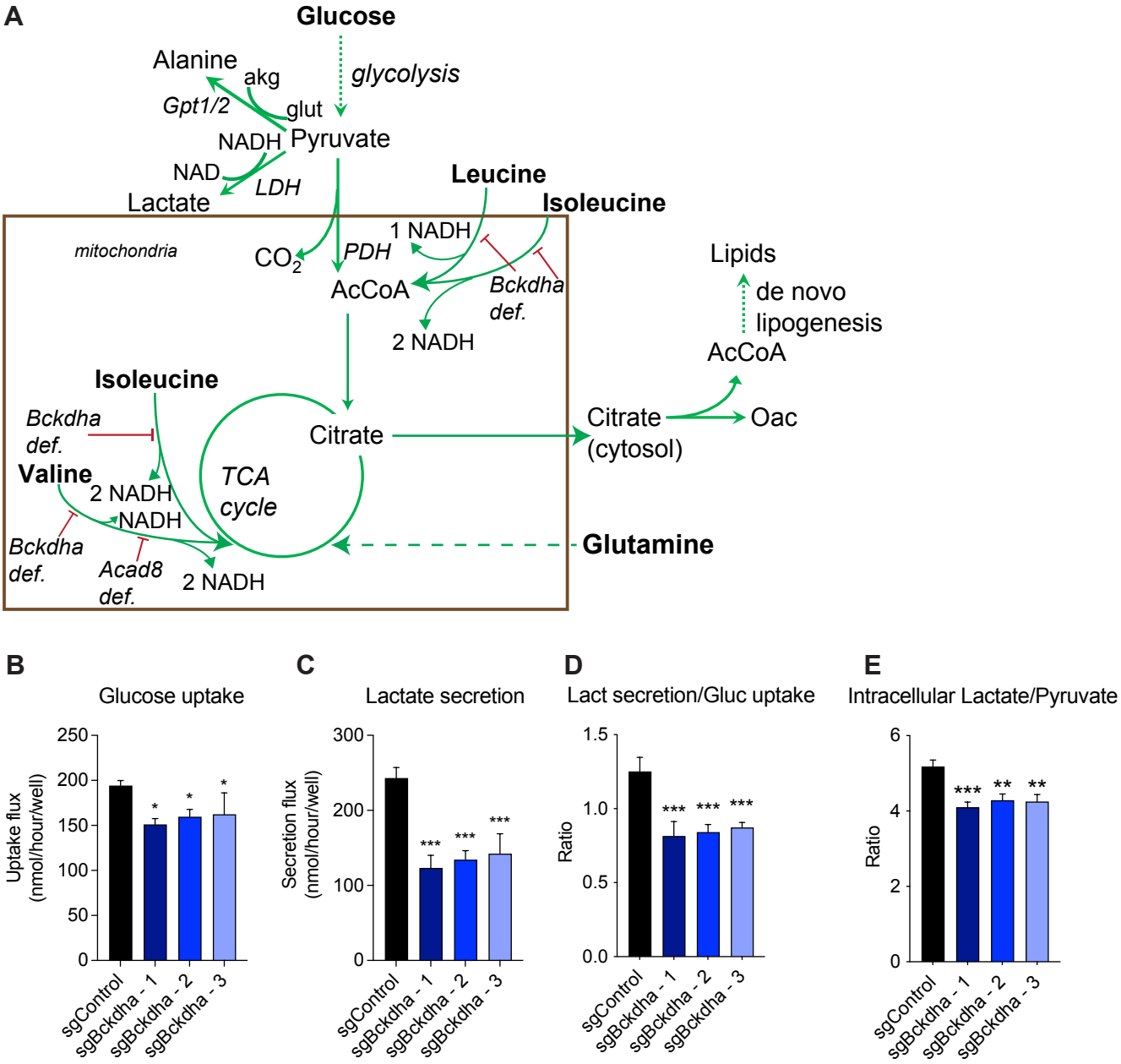


A. Simplified metabolic map of central carbon metabolism
B. Molar amount of glucose uptake in Control or Bckdha-deficient adipocytes over 48 hours
C. Molar amount of lactate secretion in Control or Bckdha-deficient adipocytes over 48 hours
C. Ratio of lactate secretion to glucose uptake after 48 hours
D. Intracellular lactate to pyruvate ratio

Data are presented as means ± SD (B-E) with three cellular replicates. One-way ANOVA with Dunnett's correction for multiple comparisons (B-E). Significance in all is compared to sgControl.
Results are depicted from one representative experiment which was repeated independently at least three times.
*p<0.05, **p<0.01, ***p<0.001.

## Figure 4
## Respiration is negatively impacted by Bckdha deficiency

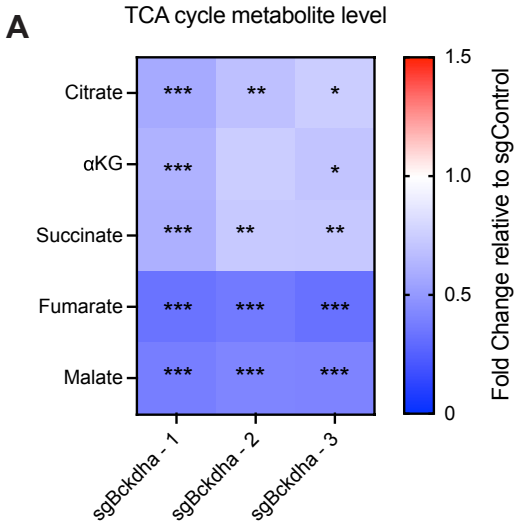


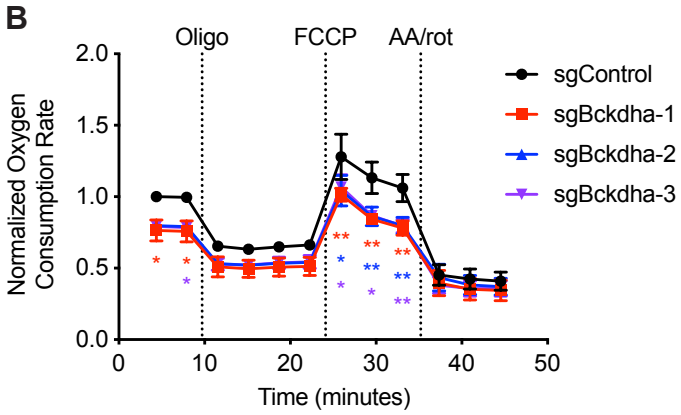


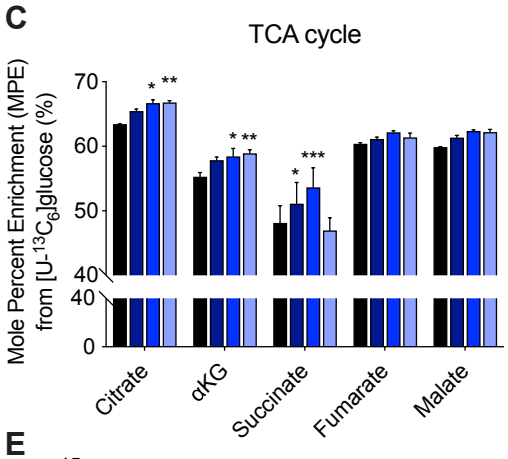


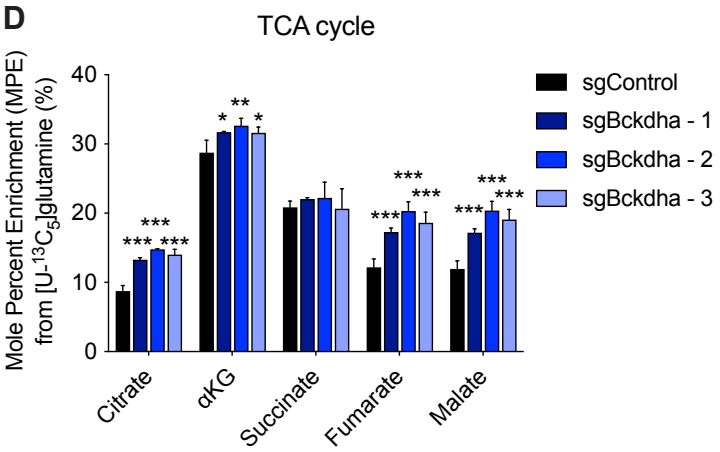


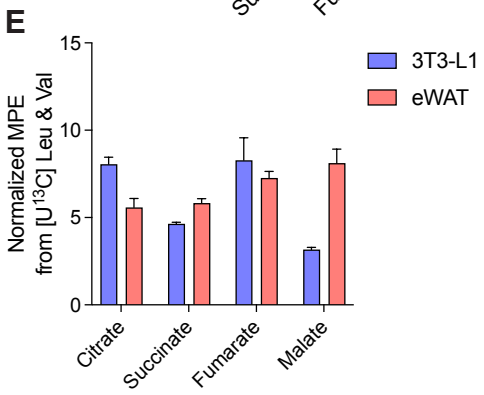


A. Relative abundance of TCA cycle intermediates in Bckdha-deficient adipocytes normalized to sgControl adipocytes
B. Normalized oxygen consumption rate of 3T3-L1 Control or Bckdha deficient adipocytes treated with the indicated pharmacological inhibitors (n=3 experiments internally normalized to sgControl)
C. Mole percent enrichment (MPE) of TCA cycle intermediates after 48 hours of incubation with [U-13C6]glucose
D. MPE of TCA cycle intermediates after 48 hours of incubation with [U-13C5]glutamine
E. Normalized MPE from dual [U-13C6]leucine and [U-13C5]valine tracing in cultured 3T3-L1 adipocytes and mice epididymal white adipose tissue (eWAT) after 21 days of labeled chow feeding

Data are presented as means ± SEM with six cellular replicates (B), means ± SD with three cellular replicates (C-D), or means ± SEM with seven tissue replicates and three cellular replicates (E). Significance in all is compared to sgControl. Results are depicted from one representative experiment which was repeated independently at least three times. *p<0.05, **p<0.01, ***p<0.001.

## Figure 5
## Altering BCAA catabolism alters fatty acid diversity

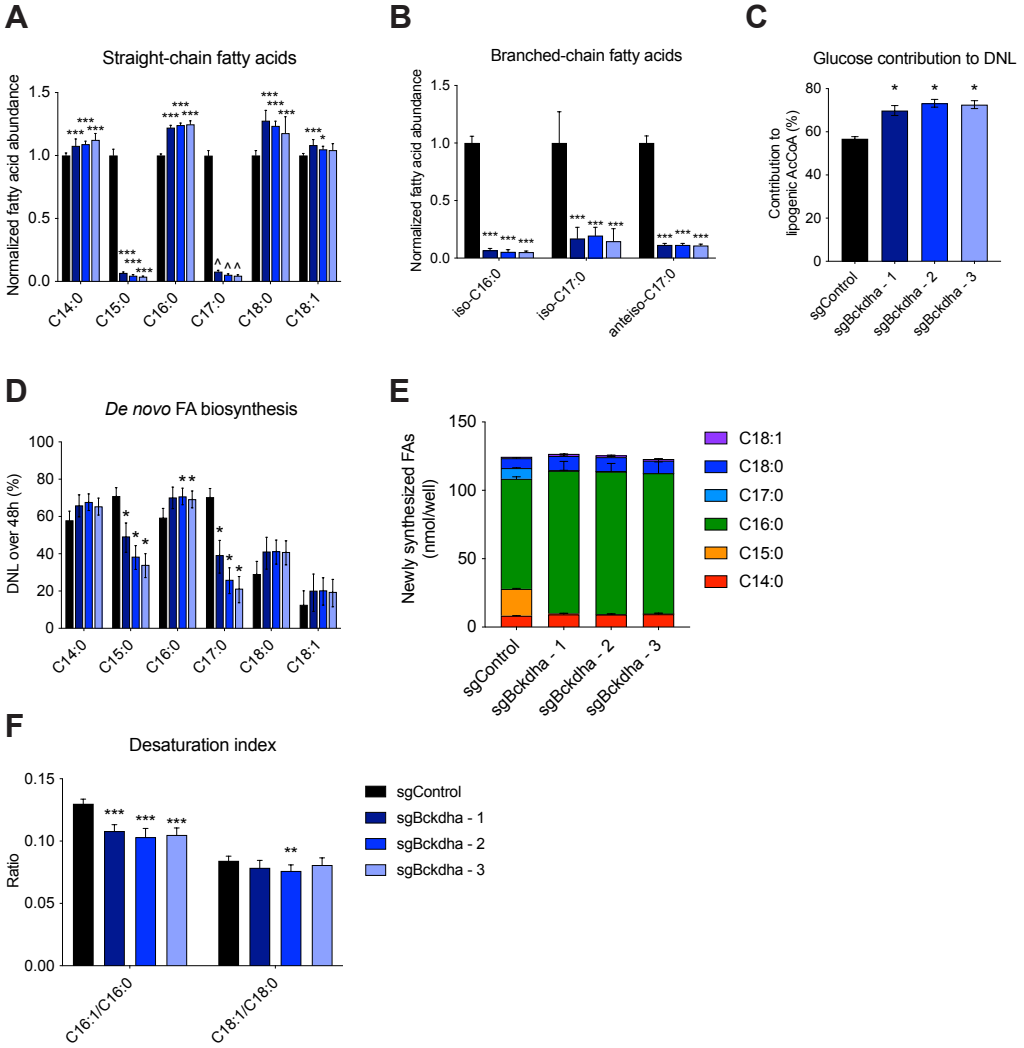


A. Relative fold change in total odd- and even- straight-chain fatty acids in Bckdha deficient 3T3-L1 adipocytes normalized to Control adipocytes.
B. Relative fold change in total branched-chain fatty acids (BCFAs) in Bckdha deficient 3T3-L1 adipocytes normalized to Control adipocytes.
C. Contribution of [U-13C6]glucose to the lipogenic AcCoA pool used for de novo lipogenesis (DNL)
D. Percent of fatty acids derived from de novo lipogenesis in Control and Bckdha deficient 3T3-L1 adipocytes over 48 hours obtained via isotopomer spectral analysis (ISA).
E. Molar amount of indicated fatty acids synthesized over 48 hours obtained by combining individual FA DNL values with pool size.
F. Desaturation index in Control and Bckdha deficient 3T3-L1 adipocytes.

Data are presented as means ± SD (A, B, F), means ± 95% C.I. (C-D), or means ± SEM (E) with three cellular replicates. Two-way ANOVA (A-B, F) or one-way ANOVA of the total values (E) all with Dunnett's correction for multiple comparisons and non-overlapping 95% C.I. (C, D). Significance in all is compared to sgControl. Results are depicted from one representative experiment which was repeated independently at least three times.
*p<0.05, **p<0.01, ***p<0.001.

**Figure 6**

**Metabolic flux analysis reveals significant reprogramming of glycolysis and TCA metabolism**

**A**

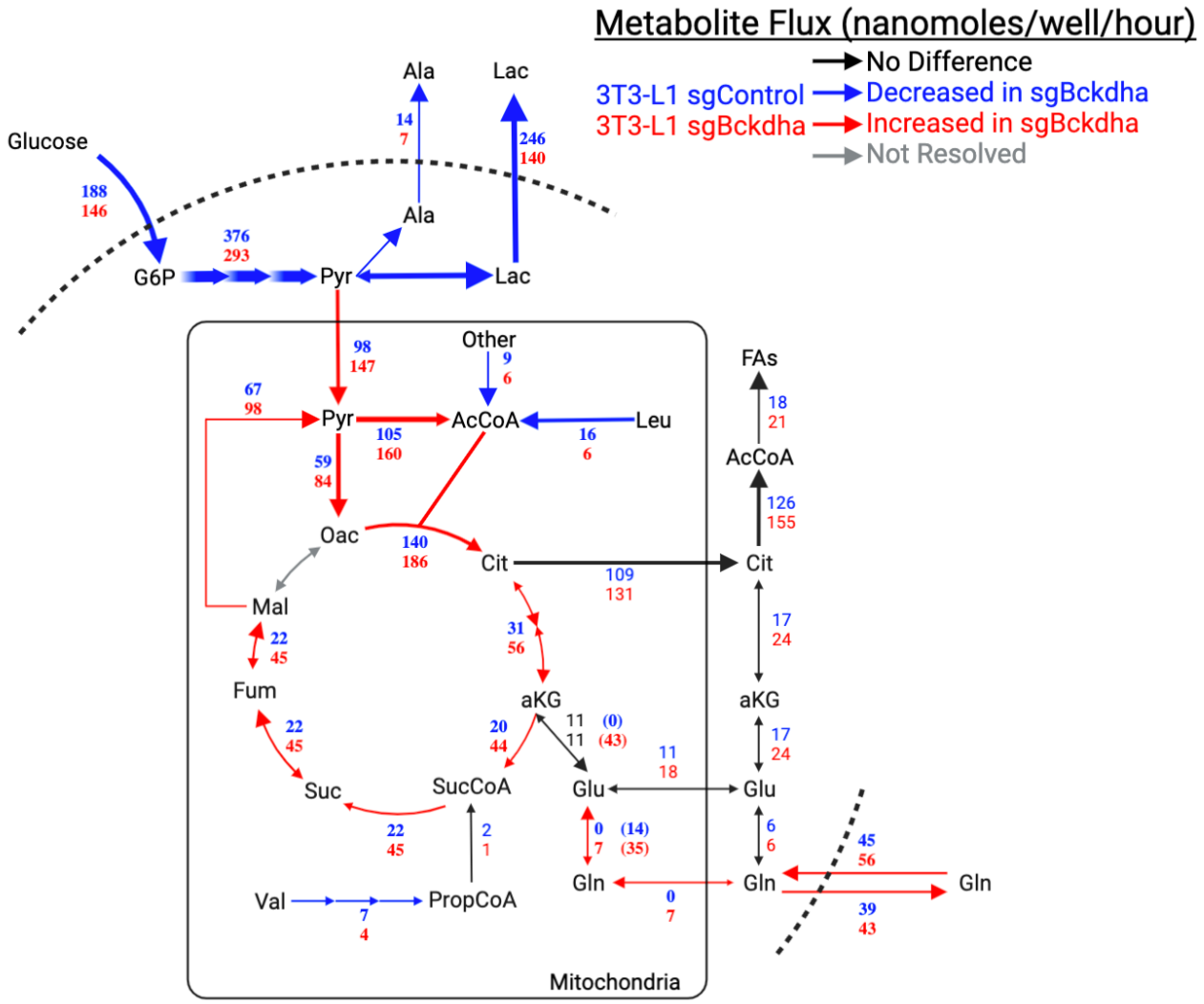


A. Map of core MFA model. Values are presented as flux (exchange flux). Blue text is sgControl, red text is sgBckdha. Blue arrows indicate a flux is decreased in sgBckdha compared to sgControl, while a red arrow indicates an increase in flux in sgBckdha. Bold text indicates significantly different reactions.

## Figure 7
## Acad8 deficiency impacts anaplerosis and alters OCFA and BCFA accumulation

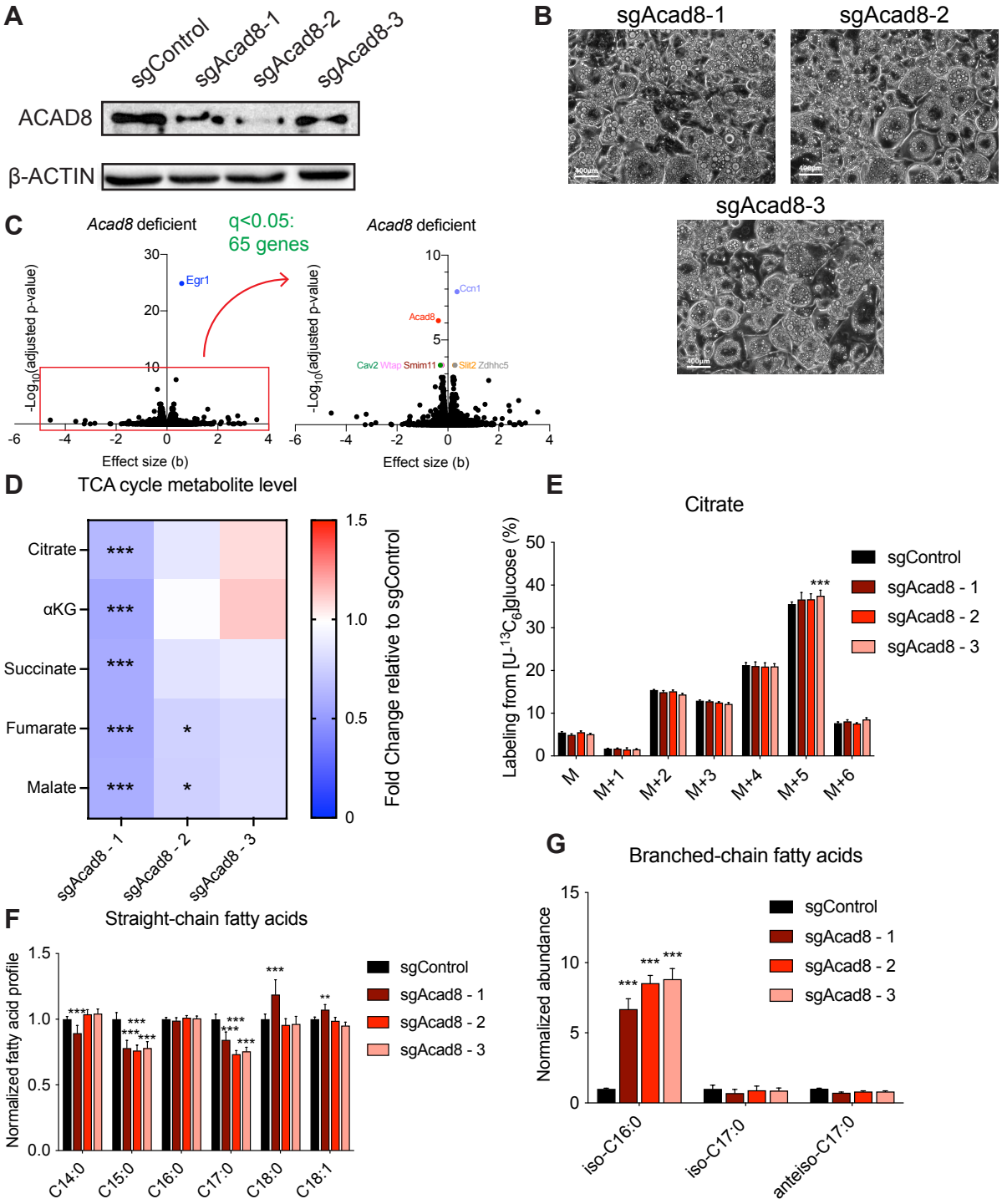


A. Western blot of Acad8 and Actin
B. Brightfield images of differentiated Control and sgAcad8 adipocytes 7 days post-induction of differentiation (scale bar = 400μm)
C. Volcano plots of differentially expressed genes in Acad8 deficient adipocytes compared to Control adipocytes
D. Heat map of the fold change of the abundance of intracellular TCA cycle intermediates in Bckdha deficient adipocytes normalized to sgControl
E. Citrate mass isotopomer distribution (MID) after 48 hours of incubation with [U-13C6]glucose
F. Relative fold change in total odd- and even- straight-chain fatty acids in Acad8 deficient 3T3-L1 adipocytes normalized to Control adipocytes.
G. Relative fold change in total branched-chain fatty acids (BCFAs) in Acad8 deficient 3T3-L1 adipocytes normalized to Control adipocytes.
Data are presented as means ± SD (E-G) with three cellular replicates. Two-way ANOVA with Dunnett's correction for multiple comparisons (E-G). Significance in all is compared to sgControl. Results are depicted from one representative experiment which was repeated independently at least three times. *p<0.05, **p<0.01, ***p<0.001.

## Supplementary Figure 1
## Bckdha deficiency alters BCKA levels and amino acid metabolism

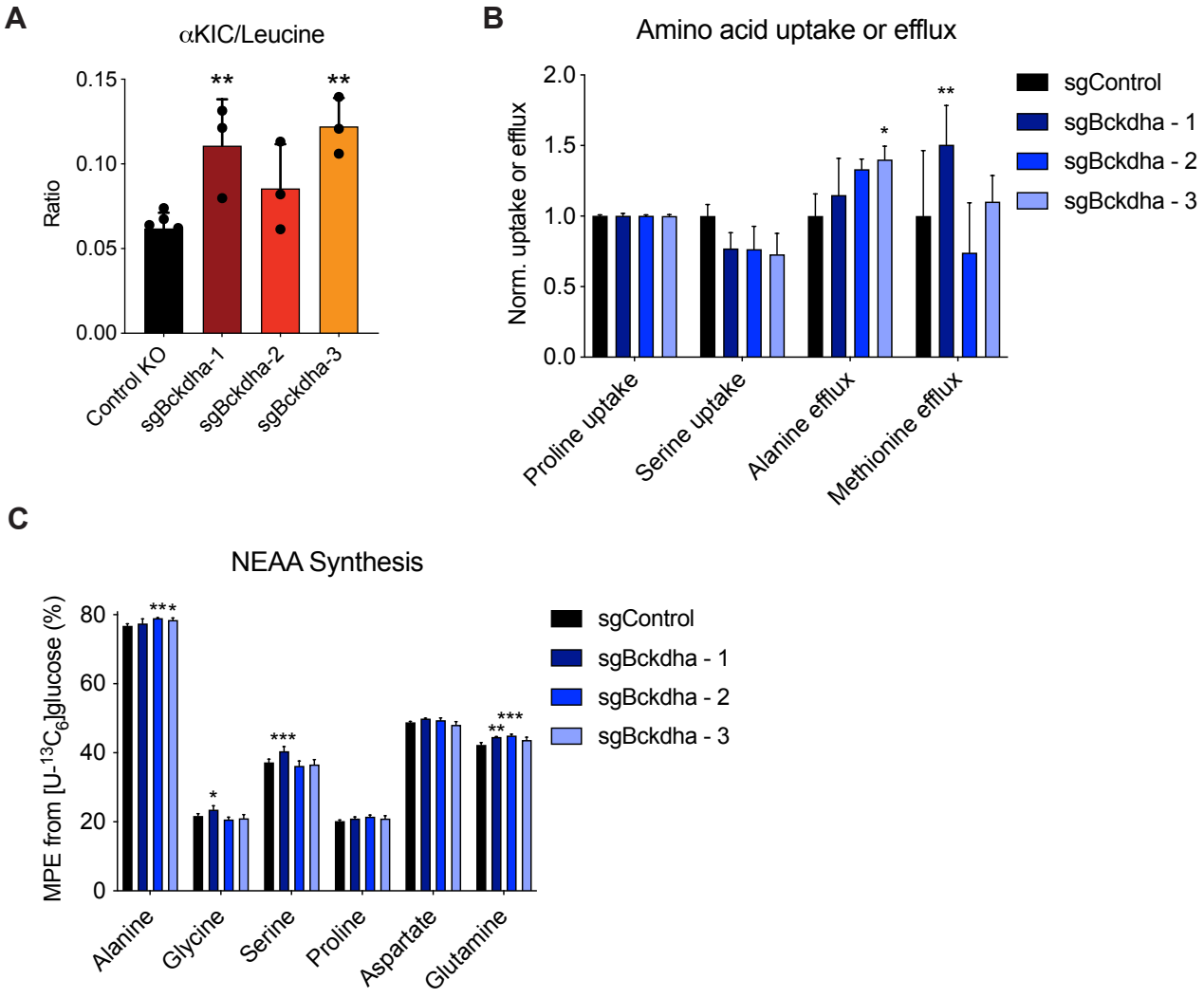


A. Ratio of α-ketoisocaproate (α-KIC) to leucine in Control and Bckdha deficient adipocytes
B. Normalized relative uptake or efflux of amino acids in Control and Bckdha deficient adipocytes
C. Mole percent enrichment (MPE) of non-essential amino acids alanine, glycine, serine, proline, aspartate, and glutamine from [U-13C6]glucose

Data are presented as means ± SD (A-C) with three cellular replicates. One-way ANOVA (A) or two-way ANOVA (B-C). Significance in all is compared to sgControl. Results are depicted from one representative experiment which was repeated independently at least three times.
*p<0.05, **p<0.01, ***p<0.001.

## Supplementary Figure 2
## Bckdha deficiency alters transcription and glucose metabolism without affecting mitochondrial number

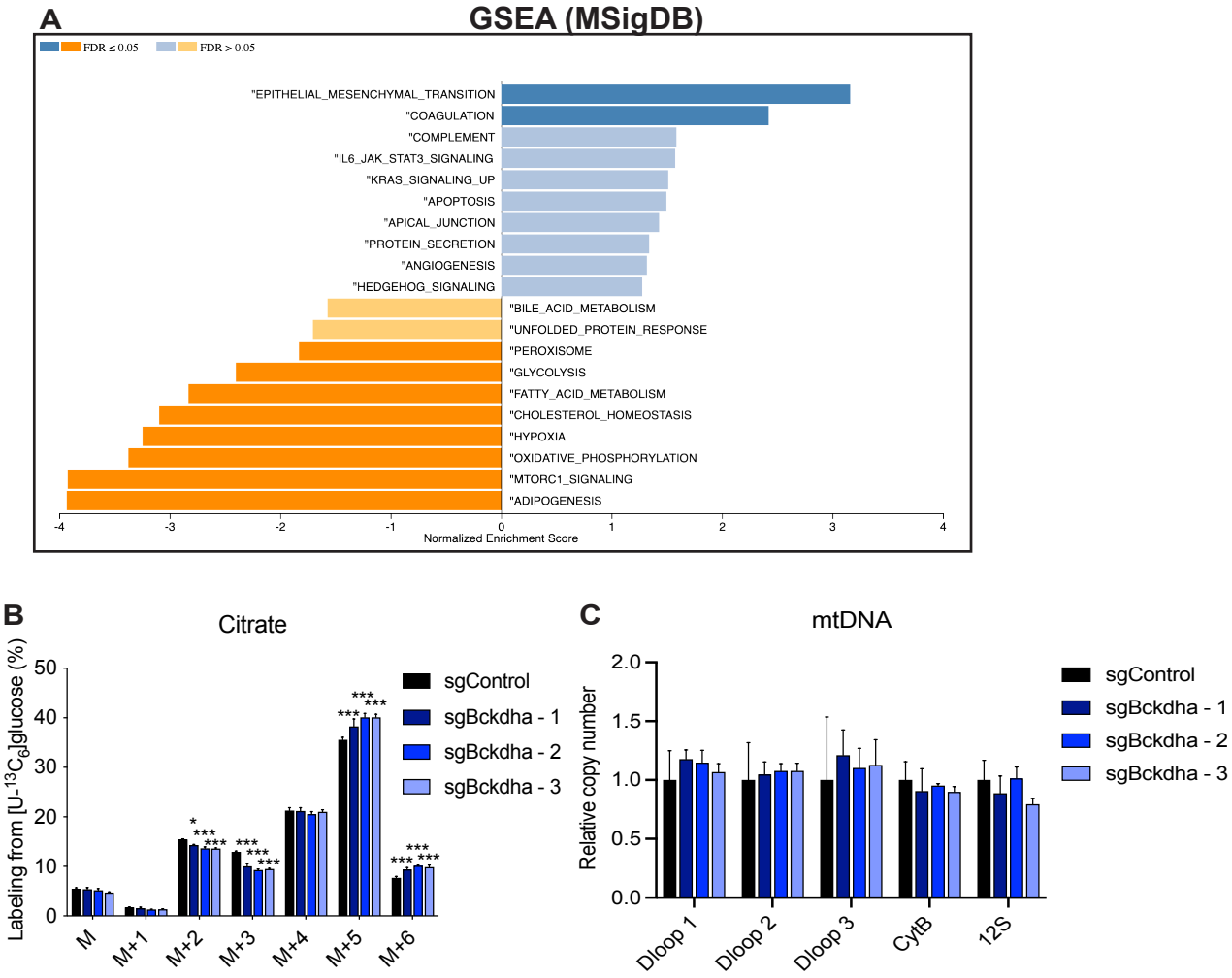


A. Gene set enrichment analysis of Bckdha deficient adipocytes generated using WEB-based GEne SeT AnaLysis Toolkit (WebGestalt) using the MsigDB biological processes hallmarks database
B. Citrate mass isotopomer distribution (MID) after 48 hours of incubation with [U-13C6]glucose
C. Normalized gene expression of mitochondrial DNA markers in Control and Bckdha deficient adipocytes

Data are presented as means ± SD (B, C) with three cellular replicates. Two-way ANOVA (B, C). Significance in all is compared to sgControl. Results are depicted from one representative experiment which was repeated independently at least three times.
*p<0.05, **p<0.01, ***p<0.001.